# Enhancement of Corrosion Protection Effect of Poly(styrene-*co*-acrylonitrile) by the Incorporation of Nanolayers of Montmorillonite Clay into Copolymer Matrix

**Jui-Ming Yeh, Shir-Joe Liou, Hsin-Jung Lu, Hsi-Ya Huang**

*Department of Chemistry and Center for Nanotechnology at CYCU, Chung-Yuan Christian University, Chung Li 320, Taiwan, Republic of China*

Received 10 March 2003; accepted 17 October 2003

**ABSTRACT:** A series of polymer–clay nanocomposite (PCN) materials that consisted of poly(styrene-*co*-acrylonitrile) (PSAN) and layered montmorillonite (MMT) clay were successfully prepared by effectively dispersing the inorganic nanolayers of MMT clay into the organic PSAN matrix by a conventional *in situ* thermal polymerization. First of all, organic styrene and AN monomers at a specific feeding ratio were simultaneously intercalated into the interlayer regions of organophilic clay hosts and followed by a typical free-radical polymerization with benzyl peroxide as initiator. The as-synthesized PCN materials were subsequently characterized by FTIR spectroscopy, wide-angle powder X-ray diffraction, and transmission electron microscopy. The as-prepared PCN materials, in the form of coatings, incorporated with low clay loading (e.g., 1 wt %) on cold-rolled steel, were found to be much superior in corrosion protection over those of bulk PSAN based on a series of standard electrochemical measurements of corrosion potential, polarization resistance, and corrosion current in 5 wt % aqueous NaCl electrolyte. Molecular weights of PSAN extracted from PCN materials and bulk PSAN were determined by gel permeation chromatography with THF as eluant. Effects of the material composition on the molecular barrier and thermal stability of PSAN along with PCN materials, in the form of both membrane and fine powder, were also studied by molecular permeability analysis, differential scanning calorimetry, and thermogravimetric analysis, respectively.
© 2004 Wiley Periodicals, Inc. J Appl Polym Sci 92: 2269–2277, 2004

**Key words:** corrosion; clay; montmorillonite; nanocomposites; coatings

## INTRODUCTION

Corrosion control is an important subject of increasing interest to the modern metallic finishing industry. Many organic and/or polymeric coatings are designed to protect a metal from in-service corrosion. Most finishing processes require the substrate surface to be free of contamination by corrosion products. Yet, many process solutions themselves are potentially corrosive. Even though highly corrosion resistant finishes have been created and process baths are generally chosen and used in a manner that minimizes substrate degradation, better methods of overcoming most corrosion problems are continually being developed.

A considerable number of coating materials for corrosion protection of metal surfaces have been reported. Currently, one of the standard industrial practices is to treat and/or coat the surface of metals with chromium-containing compounds. However, the concern on the known adverse health and environmental effects of chromium compounds persists. In the past decades, the use of electroactive organic polymers,[1–5] such as polyaniline, as corrosion protection coatings has been explored for the potential replacements of chromium-containing materials.

On the other hand, organic–inorganic nanocomposite materials continue to be the focus of extensive and intensive research interests because of their unusual hybrid properties, which are attributed to the interaction between the components combining at the molecular level. Nanocomposites based on polymers and inorganic clay minerals are a promising system because the clays are characterized by a high aspect ratio and a platelike morphology and can be used to boost the physical properties (e.g., thermal stability,[6] mechanical strength,[7] fire retardancy,[8] and gas barrier[9]) of bulk polymers.

We found that dispersing the nanolayers of montmorillonite clay into a polyaniline matrix, to increase the tortuosity of the diffusion pathway of oxygen and water, can effectively enhance the corrosion-protection effect of bulk polyaniline.[10] Similar situations are also found in both poly(methyl methacrylate)–clay[11] and poly(orthoethoxyaniline)–clay[12] nanocomposite systems.

*Correspondence to:* J.-M. Yeh (juiming@cycu.edu.tw).
Contract grant sponsor: NSC; contract grant number: 90-2113-M-033-010.

Journal of Applied Polymer Science, Vol. 92, 2269–2277 (2004)
© 2004 Wiley Periodicals, Inc.

Lee et al.[13] reported on the preparation and properties of poly(styrene-*co*-acrylontrile) (PSAN)–clay nanocomposite materials by emulsion polymerization. However, the corrosion-protection properties of PSAN–clay nanocomposite materials have yet to be reported. Therefore, in this article, we concentrate on the corrosion-protection property studies of PSAN–clay nanocomposite materials, prepared from *in situ* polymerization, in the form of a coating on a metallic surface in saline. The as-prepared nanocomposites were characterized by FTIR, wide-angle powder X-ray diffraction (XRD), and TEM. The molecular weights of PSAN extracted from polymer–clay nanocomposite (PCN) materials and bulk PSAN are determined by gel permeation chromatography (GPC) with THF as eluant. Effects of the material composition on the molecular barrier and thermal stability of PSAN along with PCN materials, in the form of both membrane and fine powder, are also investigated by molecular permeability analysis (GPA), differential scanning calorimetry (DSC), and thermogravimetric analysis (TGA), respectively.

## EXPERIMENTAL

### Chemicals and instrumentation

Polystyrene (MW = 280,000; Aldrich Chemical, Milwaukee, WI), styrene (99%; Aldrich, Switzerland), acrylonitrile (AN, 99%; Aldrich), benzoyl peroxide (98%; Riedel-de Haën, Seelze, Germany), *N*-methyl-2-pyrrolidone (NMP, 99.6%; Tedia, Ohio), tetrahydrofuran (THF) for GPC (99.8%; Fisher Scientific, Pittsburgh, PA), lithium chloride (99%; Acros Organics, Morris Plains, NJ), hydrochloric acid (37%; Riedel-de Haën, Seelze, Germany), THF for reagent (99%; Riedel-de Haën), and methanol (80%; Riedel-de Haën) were used as received without further purification. [2-(Dimethylamino)ethyl]–triphenylphosphonium bromide (97%; Aldrich), $Br^{-}P^{+}(Ph)_3—CH_2—CH_2—N(CH_3)_2$, was used as an intercalating agent (97%; Aldrich, Milwaukee, WI). The montmorillonite clay, supplied by Industrial Technology Research Institute (ITRI), had a unit cell formula $Na^{+}_{0.31}[Al_{1.67}Mg_{0.33}]Si_4O_{10}(OH)_2 \cdot 5.8H_2O$ and a CEC (cationic exchange capacity) value of 95 meq/100 g.

Wide-angle X-ray diffraction study of the samples was performed on a Rigaku D/MAX-3C OD-2988N X-ray diffractometer (Rigaku, Japan) with copper target and Ni filter at a scanning rate of 2°/min. The samples for transmission electron microscopy (TEM) study was first prepared by mixing powder of PCN materials into epoxy resin capsules followed by curing the epoxy resin at 100°C for 24 h in a vacuum oven. Then the cured epoxy resin containing PCN materials were microtomed with a Reichert-Jung Ultracut-E into slices 60–90 nm thick. Subsequently, one layer of carbon about 10 nm thick was deposited on these slices on mesh 100 copper nets for TEM observations on a JEOL-200FX (JEOL, Tokyo, Japan) with an acceleration voltage of 120 kV. FTIR spectra were recorded on pressed KBr pellets using a Bio-Rad FTS-7 FTIR spectrometer (Bio-Rad, Hercules, CA). Elemental analysis was performed on a Perkin–Elmer series II CHNS/O 2400 (Perkin Elmer Cetus Instruments, Norwalk, CT). A Perkin–Elmer thermal analysis system, equipped with model 7 DSC and model 7/DX TGA, was used for the thermal analyses under nitrogen gas flow. The programmed heating rate was 20°C/min in most cases. The molecular weight of neat and extracted polymers was determined by GPC. A Waters GPC model 2 II (Waters Chromatography Division/Millipore, Milford, MA), equipped with a model 590 programmable solvent delivery module, a differential refractometer detector, and a ultrastyragel linear packed column, was used to perform the GPC studies. Temperatures of the GPC column and detector were kept at 35°C. THF (Aldrich) was employed as an eluant at a flow rate of 1.0 mL/min. Molecular weights of the standard polystyrene samples (Waters) were 5000, 35,000, and 470,000.

Corrosion potential, polarization resistance, and corrosion current measurements on sample-coated CRS coupons were performed on a VoltaLab 21 potentiostat/galvanostat in a standard corrosion cell, equipped with two graphite rod counter electrodes and a saturated calomel electrode (SCE) as well as the working electrode. The molecular weights of polymers extracted from all composite samples as well as bulk PSAN were determined on a Perkin–Elmer model TC4 equipped with a model 590 programmable solvent delivery module, a differential refractometer detector and a Styragel HT column with THF as eluant and monodispersed polystyrenes as calibration standards. A Yanagimoto Co. (Japan) gas permeability analyzer (model GTR 10) was used to perform the permeation experiment of oxygen gas and water vapor.

### Synthesis of PSAN

A representative process of synthesizing PSAN was as follows: 10.4 g (0.1 mmol) of styrene, 5.4g (0.1 mmol) of acrylonitrile, 0.242 g (0.001 mmol) of benzoyl peroxide (BPO), and 100 mL of dry THF were charged to a 250-mL three-neck round-bottom flask connected with a condenser, a thermometer, and nitrogen gas inlet/outlet. Nitrogen gas was bubbled into the flask throughout the reaction. Under magnetic stirring, the solution was heated to 85°C and maintained for 24 h. The reaction mixture solution was then poured into about 500 mL of methanol to precipitate the polymer. After filtration, the polymer was dissolved in 60 mL of dry THF after which it was reprecipitated in 500 mL of

methanol. The purification procedure was repeated at least twice, and the purified polymer was then dried under vacuum at room temperature for 48 h. The as-prepared polymer (12.5 g) was obtained in about 80% yield.

### Preparation of organoplilic clay

Organophilic clay can be successfully prepared by a cationic-exchange reaction between the sodium cations of MMT clay and quaternary alkylphosphonium cations of $Br^{-}P^{+}(Ph)_3—CH_2—CH_2—N(CH_3)_2$, [2-(dimethylamino)ethyl]–triphenylphosphonium bromide, as intercalating agent. The equation for calculating the intercalating agent used for cationic-exchange reaction is as follows:

$$95/100 \times 5\ \text{g(for clay)} \times 1.2 = (X/\text{MW of intercalating agent}) \times 1 \times 1000$$

where $X$ represents the amount of intercalating agent used; 95/100 represents the CEC value per 100 g of MMT clay; and 1.2 (>1) indicates the excess amount of intercalating agent used. Typically, 5 g of MMT clay with a CEC value of 95 meq/100 g was dispersed in 400 mL distilled water (beaker A) under magnetic stirring at room temperature overnight. A separate solution containing an excess amount of intercalating agent (2.45 g) was added to 30 mL of distilled water (beaker B) under magnetic stirring, followed by addition of 1*M* HCl aqueous solution to adjust the pH value to approximately 3–4. After stirring for 1 h, the protonated amino acid solution (beaker B) was added, at a rate of approximately 10 mL/min with vigorous stirring, to the MMT suspension (beaker A). The mixture was stirred overnight at room temperature. The organophilic clay was recovered by ultracentrifugating (9000 rpm, 30 min) and filtering the solution in a Buchner funnel. Purification of products was performed through washing with distilled water (because the intercalating agent is water soluble) and filtering samples repeatedly for at least three times to remove any excess of phosphonium ions.

### Preparation of PSAN–clay nanocomposites by *in situ* polymerization

As a typical procedure for the preparation of the PCN materials with 1 wt % clay loading, first, an appropriate amount of organophilic clay (0.1 g) was introduced into 100 mL of THF under magnetic stirring overnight at room temperature. Styrene monomers (6.52 g, 63 mmol) and acrylonitrile monomers (3.38 g, 63 mmol) were subsequently added to the solution, which was stirred for another 24 h. Upon addition of BPO (0.0758 g), the solution was stirred for 24 h at 85°C under $N_2$ atmosphere. The as-synthesized nanocomposite precipitates were then obtained by precipitating from an excess amount of methanol (500 mL) and subsequent drying under dynamic vacuum at room temperature for 48 h.

### Polymer recovery (extraction)

To determine the degree of polymerization of feeding monomers, which diffused into the interlayer regions of organophilic clay, a reverse cationic-exchange reaction was usually used to separate the bound polymer from the inorganic component in the nanocomposite.[14] As a typical extraction procedure, 2 g of fine powder of as-synthesized PCN fine powders was dissolved in about 100 mL of THF (beaker A). Separately, a 10 mL stock solution of 1 wt % $LiCl_{(s)}$ in THF was prepared (beaker B). Both beakers were under magnetic stirring for 3–4 h at room temperature. After combining the contents of the two beakers, the mixture was stirred overnight, followed by Soxhlet extraction at 80°C for 24 h. The extract solution was then poured into an excess amount of methanol to precipitate the polymer. After filtration, the polymer was dried under vacuum at room temperature for 48 h. Molecular weights of both extracted and bulk PSAN were determined by GPC analyses with THF as eluant.

### Preparation of coatings and electrochemical measurements

The PSAN and PCN fine powder were dissolved in NMP to give typically 2 wt % solutions for the film formation. The solutions were then cast dropwise onto cold-rolled steel (CRS) coupons (1.0 × 1.0 cm) followed by drying in air for 24 h at 40°C to give coatings of about 25 $\mu$m thickness, measured by a digimatic micrometer (Mitutoyo, Japan),. The coating ability of PCN on CRS was found to be similar to that of bulk PSAN. The coated and uncoated coupons were then mounted onto the working electrode so that only the coated side of the coupon was in direct contact with the electrolyte. The edges of the coupons were sealed with superfast epoxy cement (SPAR®). All the electrochemical measurements of corrosion potential, polarization resistance, and corrosion current were performed on a VoltaLab model 21 potentiostat/galvanostat and repeated at least three times. The electrolyte was NaCl (5 wt %) aqueous solution. The open circuit potential (OCP) at the equilibrium state of the system was recorded as the corrosion potential ($E_{corr}$ in V versus SCE). The polarization resistance ($R_p$ in $\Omega/cm^2$) was measured by sweeping the applied potential from 20 mV below to 20 mV above the $E_{corr}$ at a scan rate of 500 mV/min and recording the corresponding current change. The $R_p$ value was ob-

**TABLE I**
**Relations of the Composition of PSA–MMT Clay Nanocomposite Materials with the $E_{corr}$, $R_p$, $I_{corr}$, and $R_{corr}$ Measured from Electrochemical Methods**

| Compound code | Feed composition (wt %) | | Inorganic content found in product[a] (wt %) | Electrochemical corrosion measurements[b] | | | | |
|---|---|---|---|---|---|---|---|---|
| | PSAN | MMT | | $E_{corr}$ (mV) | $R_p$ (k$\Omega$/cm$^2$) | $I_{corr}$ (nA/cm$^2$) | $R_{corr}$ (MPY) | Thickness ($\mu$m) |
| Bare | — | — | — | −604 | 2.7 | $1.9 \times 10^4$ | 36.7 | — |
| PSA | 100 | 0 | 0 | −490 | $1.3 \times 10^2$ | $6.1 \times 10^2$ | 1.17 | 24 |
| CLSA1 | 99 | 1 | 0.9 | −449 | $1.4 \times 10^2$ | $3.4 \times 10^2$ | 0.65 | 25 |
| CLSA3 | 97 | 3 | 3.6 | −403 | $3.3 \times 10^2$ | $2.5 \times 10^2$ | 0.48 | 27 |
| CLSA5 | 95 | 5 | 7.1 | −381 | $3.8 \times 10^2$ | $1.7 \times 10^2$ | 0.33 | 24 |
| CLSA10 | 90 | 10 | 9.4 | −314 | $5.9 \times 10^2$ | $9.5 \times 10^1$ | 0.18 | 26 |

[a] As determined from TGA measurements.
[b] Saturated calomel electrode was used as reference electrode.

tained from the slope of the potential–current plot. The Tafel plots were obtained by scanning the potential from 250 mV below to 250 mV above the $E_{corr}$ at a scan rate of 500 mV/min. The corrosion current ($I_{corr}$) was determined through superimposing a straight line along the linear portion of the cathodic or anodic curve and extrapolating it through $E_{corr}$. The corrosion rate [$R_{corr}$, in milli-inches per year (MPY)] was calculated from the following equation:

$$R_{corr}(\text{MPY}) = [0.13 I_{corr}(\text{EW})]/[Ad]$$

where EW is the equivalent weight (in g/eq), $A$ is the area (in cm$^2$), and $d$ is the density (in g/cm$^3$).

### Preparation of membranes and barrier property measurements

To enhance the mechanical strength of membrane of as-synthesized materials for molecular ($H_2O$ and $O_2$) barrier property measurements under high-pressure difference conditions, a commercial polystyrene (PS) with high molecular weight (MW = 280,000) was blended into the casting solution for film formation. Typically, 0.1 g of as-synthesized PSAN or PCN materials blended with 0.1 g of commercialized PS was dissolved in 10 mL of NMP under magnetic stirring at room temperature for 4 h. The solution was then cast onto a substrate (e.g., a microscope glass slide). The solvent was allowed to evaporate at 90–100°C under the hood for 24 h. The sample-coated glass substrate was then immersed in distilled water for 24 h to give the membrane of PSAN and PCN materials. Oxygen permeabilities of the membrane were determined by using the Yanco GTR-10 gas permeability analyzer. The gas permeability was measured by the following equation:

$$P = l/(p_1 - p_2) \times \frac{q/t}{A}$$

where $P$ is the gas permeability [cm$^3$(STP) cm/cm$^2$ s$^{-1}$ cmHg$^{-1}$]; $q/t$ is the volumetric flow rate of the gas permeate [cm$^3$(STP)/s]; $l$ is the membrane thickness (cm); $A$ is the effective membrane area (cm$^2$); and $p_1$ and $p_2$ are the pressures (cmHg) on the high-pressure and low-pressure sides of the membrane, respectively. The rate of transmission of $O_2$ was obtained by gas chromatography, from which the air permeability was calculated. On the other hand, water vapor permeation was performed through the same apparatus employed in our previously published articles.[12]

## RESULTS AND DISCUSSION

Montmorillonite (MMT) is a clay mineral containing stacked silicate sheets measuring about 10 Å in thickness and about 2200 Å in length,[15] characterized by a high aspect ratio and a platelike morphology. MMT has a high swelling capacity, which was important for efficient intercalation of the polymer.

As a typical procedure for preparation of the PCN materials, organophilic clay was first prepared by a cationic-exchange reaction between the sodium cations of MMT clay and alkylphosphonium ions of the intercalating agent. Organic styrene and AN monomers were subsequently intercalated into the interlayer regions of organophilic clay hosts and followed by a typical free-radical polymerization. The composition of the PCN materials was varied from 0 to 10 wt % of clay with respect to PSAN content, as summarized in Table I.

### Characterization

Representative FTIR spectra of the organophilic clay, bulk PSAN, and PCN materials are shown in Figure 1. The characteristic vibration bands of PSAN are at 1450, 1500, and 1600 cm$^{-1}$ (aromatic C═C); 700 and 750 cm$^{-1}$ (monosubst. benzene); 2240 cm$^{-1}$ (–C≡N stretching); and those of MMT clay are shown at 1040

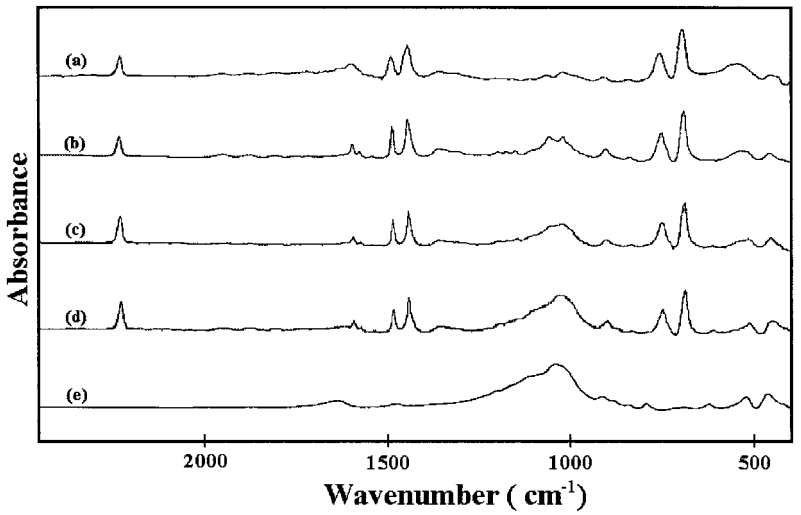


**Figure 1** FTIR spectra of (a) PSAN, (b) CLSA1, (c) CLSA5, (d) CLSA10, and (e) organophilic clay.

(Si—O), 520 (Al—O), and 480 $cm^{-1}$ (Mg—O).[10–12] As the loading of MMT clay was increased, the intensities of MMT clay bands became stronger in the FTIR spectra of PCN materials. Figure 2 shows the wide-angle powder XRD patterns of organophilic clay and a series of PCN materials. For CLSA1, there was a lack of any diffraction peak at $2\theta$ = 2–10°, as opposed to the diffraction peak at $2\theta = 5.91°$ ($d$ spacing = 1.49 nm) for organophilic clay, indicating the possibility of having exfoliated silicate nanolayers of organophilic clay dispersed in the PSAN matrix.

In Figure 3 the TEM of PCN materials, consisting of 5 wt % clay, reveals that the nanocomposite displayed a mixed nanomorphology. Individual silicate layers, along with two- and three-layer stacks, were found to be exfoliating in the PSAN matrix. In addition, some larger intercalated tactoids can also be identified.

### Molecular weight determination of extracted and bulk PSAN

Molecular weights of the various polymer samples recovered from the nanolayers of MMT clays were obtained by GPC analyses with THF as the eluant. GPC elution patterns of all the samples displayed a single peak, corresponding to a molecular weight

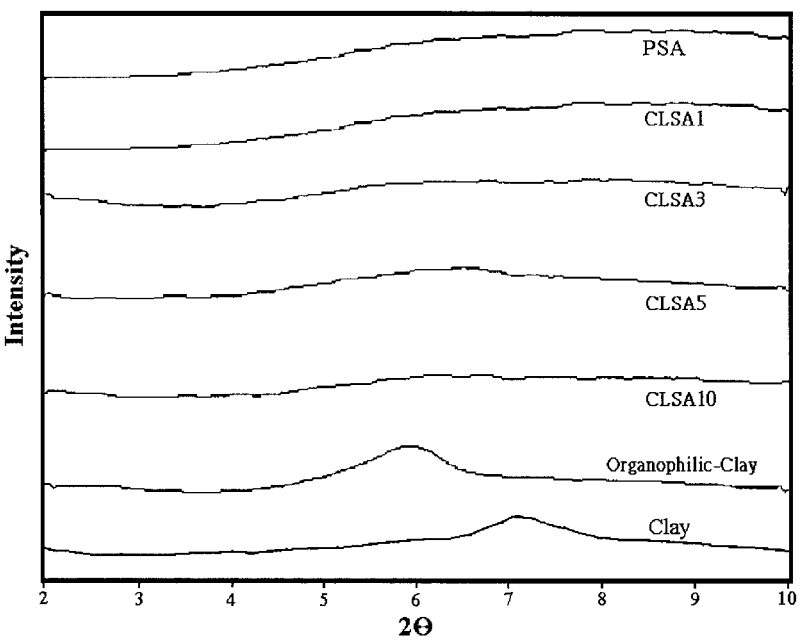


**Figure 2** Wide-angle powder X-ray diffraction patterns of organophilic clay, PSAN, and a series of PSAN–clay nanocomposite materials.

**Figure 3** Transmission electron microscopy of CLSA5.

value, as summarized in Figure 4. The molecular weights of extracted PSAN were found to be slightly lower than that of the bulk PSAN, indicating the structurally restricted polymerization situations in the intragallery region of the MMT clay and/or the nature of clay–oligomer interactions, such as adsorption, during the polymerization reaction.[16]

### Corrosion-protection performance of coatings

In this study, the corrosion-protection performance of sample-coated CRS coupons was examined by the values of corrosion potential ($E_{corr}$), polarization resistance ($R_p$), corrosion current ($I_{corr}$), and corrosion rate ($R_{corr}$), as listed in Table I. The CRS coupon coated with PSAN showed a higher $E_{corr}$ value than that of the uncoated CRS. However, it exhibited a lower $E_{corr}$ value than that of the specimen coated with PCN materials. For example, the CLSA1-coated CRS had a high corrosion potential of about −449 mV at 30 min. Even after a 5-h measurement, the potential remained at about −458 mV. Such an $E_{corr}$ value implied that the CLSA1-coated CRS showed improved anticorrosion performance toward the electrochemical corrosion compared to that of the PSAN. The CLSA1-coated CRS showed a polarization resistance ($R_p$) value of $1.4 \times 10^2$ kΩ/cm$^2$ in 5 wt % NaCl, which was about 2 orders of magnitude greater than that of the uncoated CRS. The Tafel plots for uncoated, PSAN-coated, CLSA1-coated, CLSA3-coated, CLSA5-coated, and CLSA10-coated CRS are shown in Figure 5(a)–(f), respectively. For example, the corrosion current ($I_{corr}$) of CLSA1-coated CRS was about $3.4 \times 10^2$ nA/cm$^2$, which corresponded to a corrosion rate ($R_{corr}$) of about 0.65 MPY (Table I). Moreover, the electrochemical corrosion current values of PCN materials as coatings on CRS were found to decrease gradually with further increases in clay loading. In this study, we found that the enhanced corrosion-protection effect of PSAN–clay nanocomposite coatings on a metallic surface may be attributed to the barrier effect of MMT clay platelets dispersing in composites. This barrier effect of PCN materials, compared to bulk PSAN, may be attributed to the dispersing silicate nanolayers of MMT clay in the PSAN matrix to increase the tortuosity of the diffusion pathway of $H_2O$ and $O_2$ molecules.[10–12] This can be further evidenced by the studies of the $H_2O$ vapor and $O_2$ barrier effect as discussed in the following section.

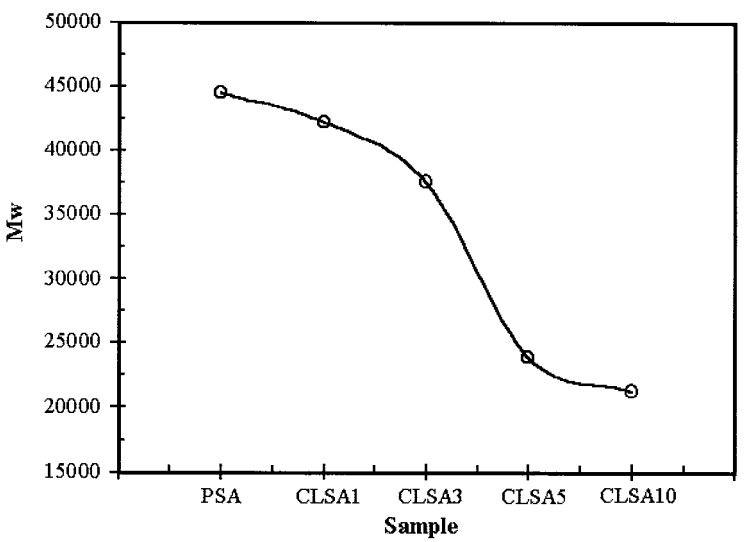


**Figure 4** GPC curves of the molecular weights of PSAN extracted from PCN materials and bulk PSAN.

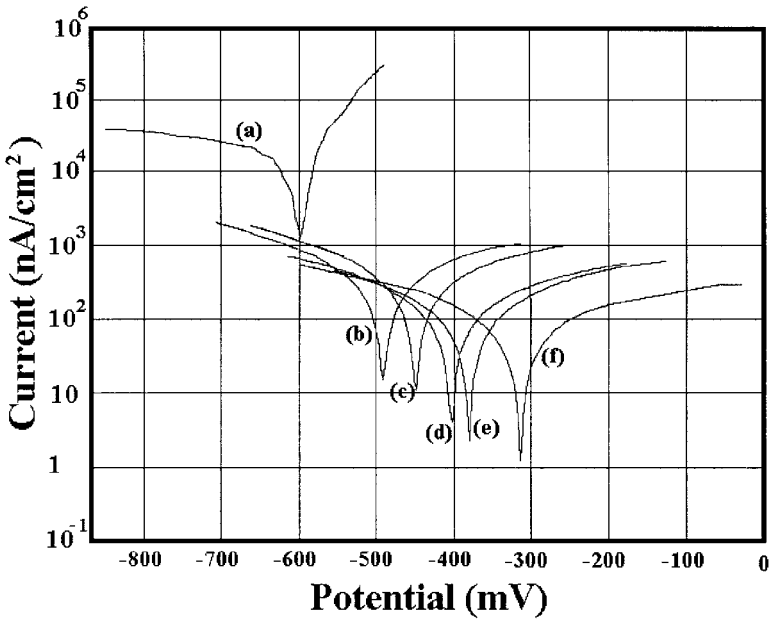


**Figure 5** Tafel plots for (a) uncoated, (b) PSAN-coated, (c) CLSA1-coated, (d) CLSA3-coated, (e) CLSA5-coated, and (f) CLSA10-coated CRS measured in 5 wt % NaCl aqueous solution.

### Molecular barrier property of membranes

The membranes of PCN materials and bulk PSAN used for the molecular barrier measurements were prepared with a film thickness of about 50 $\mu$m. Compared to PSAN, membranes of PCN materials at low clay loading (e.g., 3 wt %) showed about 30 and 72% reduction of $H_2O$ and $O_2$ permeability, respectively, as shown in Figure 6. Moreover, it should be noted that a further increase of clay loading resulted in a slightly further enhanced molecular barrier property of bulk PCN materials.

### Thermal properties of fine powders

Figure 7 shows typical TGA thermograms of weight loss as a function of temperature for PSAN and PCN materials, as measured under nitrogen gas. In general, there appear to be several stages of weight loss starting at about 290°C and ending at 800°C, which might correspond to degradation of the intercalating agent followed by the structural decomposition of the polymers. Evidently, the thermal decomposition of these PCN materials shifts toward a higher temperature range than that of PSAN, which confirms the enhance-

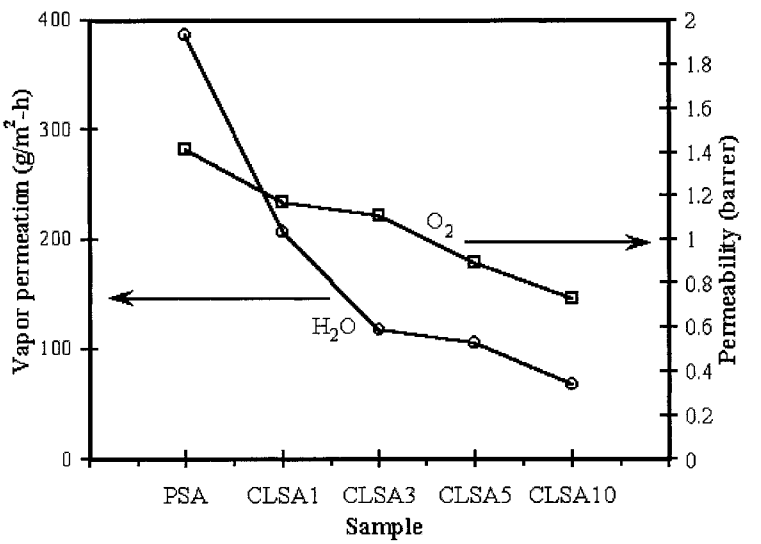


**Figure 6** Permeability of $H_2O$ and $O_2$ as a function of the MMT clay content in the PSAN–clay nanocomposite materials.

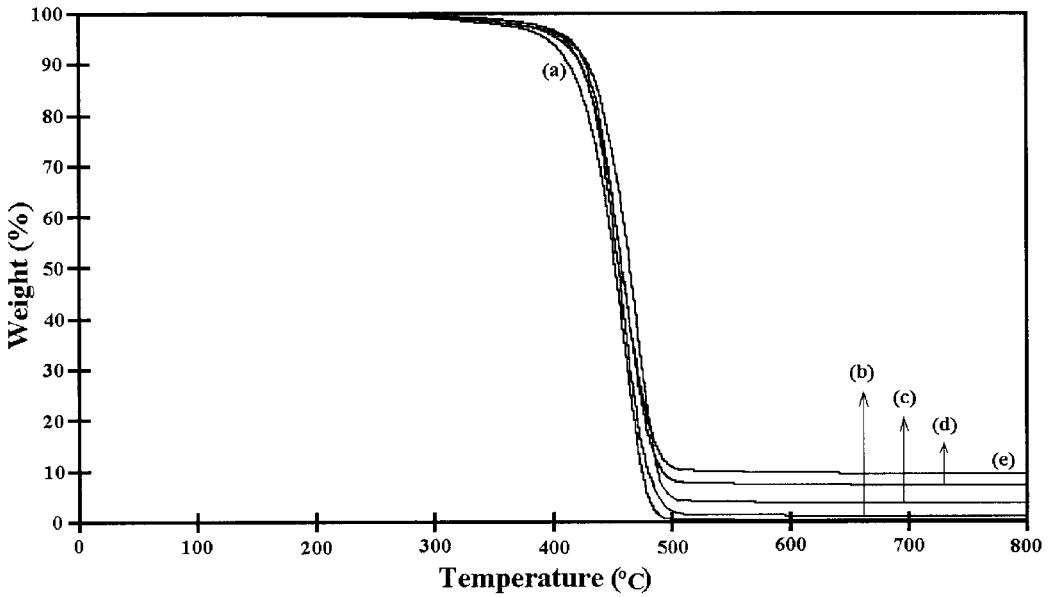


**Figure 7** TGA curves of (a) PSAN, (b) CLSA1, (c) CLSA3, (d) CLSA5, and (e) CLSA10

ment of thermal stability of intercalated PSAN.[17] After about 600°C, the curves all became flat and mainly the inorganic residue (i.e., $Al_2O_3$, MgO, $SiO_2$) remained. DSC traces of pure PSAN and PCN materials are shown in Figure 8. The pure PSAN exhibited an endotherm at 85.9°C, corresponding to the $T_g$ of PSAN. All the PCN materials showed an increased $T_g$ compared to that of pure PSAN, as shown in Figure 8. This was tentatively attributed to the confinement of the intercalated polymer chains within the clay galleries that prevented the segmental motions of the polymer chains.[11]

## CONCLUSIONS

In this study, a series of polymer–clay nanocomposite (PCN) materials were successfully prepared by effectively dispersing the inorganic nanolayers of MMT clay into an organic PSAN matrix by an *in situ* thermal polymerization. Organic styrene and acrylonitrile monomers were first intercalated simultaneously into the interlayer regions of organophilic clay hosts and followed by a typical free-radical polymerization. The as-synthesized PCN materials were subsequently characterized by FTIR, powder XRD, and TEM. PCN coatings with low clay loading (e.g., 1 wt %) on CRS were found to be substantially superior in corrosion protection over those of bulk PSAN, based on a series of electrochemical measurements of corrosion potential, polarization resistance, and corrosion current in 5 wt % aqueous NaCl electrolyte. Enhanced anticorrosion of PSAN–clay nanocomposite materials also compared to bulk PSAN might be attributed to dispersing silicate

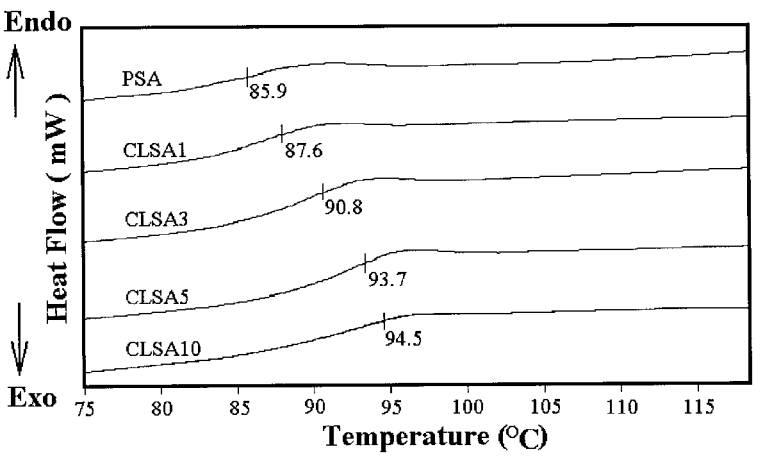


**Figure 8** DSC curves of PSAN and a series of PSAN–clay nanocomposite materials.

nanolayers of clay into the PSAN matrix to increase the tortuosity of the diffusion pathway of oxygen and water. The molecular weight of extracted PSAN was found to be slightly lower than that of the bulk PSAN, indicating the structurally restricted polymerization situations in the intragallery region of the MMT clay and/or the nature of clay–oligomer interactions, such as adsorption, during the polymerization reaction. The membrane of PCN materials at low clay loading (e.g., 3 wt %), compared to PSAN, showed about 30 and 72% reduction of $H_2O$ and $O_2$ permeability, respectively. Thermal decomposition of those PCN materials shifted toward the higher temperature range than that of PSAN based on the TGA studies, which confirmed the enhancement of thermal stability of intercalated PSAN. All the PCN materials showed an increased $T_g$ compared to that of pure PSAN based on the DSC studies. This was tentatively attributed to the confinement of the intercalated polymer chains within the clay galleries, which prevents the segmental motions of the polymer chains.

The authors gratefully acknowledge the financial support of this research by the NSC (Grant 90-2113-M-033-010).

## References

1. Deberry, D. W. J Electrochem Soc 1985, 132, 1027.
2. Wessling, B. Adv Mater 1994, 6, 226.
3. Li, P.; Tan, T.-C.; Lee, J. Y. Synth Met 1997, 88, 237.
4. Wei, Y.; Wang, J.; Jia, X.; Yeh, J.-M.; Spellane, P. Polymer 1995, 36, 4535.
5. Camalet, J. L.; Lacroix, J. C.; Aeiyach, S.; Chane-Ching, K.; Lacaze, P. C. J Electroanal Chem 1996, 416, 179.
6. Lan, T.; Kaviratna, P. D.; Pinnavaia, T. J Chem Mater 1994, 6, 573.
7. Tyan, H.-L.; Liu, Y.-C.; Wei, K.-H. Chem Mater 1999, 11, 1942.
8. Gilman, J. W.; Jackson, C. L.; Morgan, A. B.; Hayyis, R., Jr.; Manias, E.; Giannelis, E. P.; Wuthenow, M.; Hilton, D.; Phillips, S. H. Chem Mater 2000, 12, 1866.
9. Wang, Z.; Pinnavaia, T. J Chem Mater 1998, 10, 3769.
10. Yeh, J.-M.; Liou, S.-J.; Lai, C.-Y.; Wu, P.-C. Chem Mater 2001, 13, 1131.
11. Yeh, J.-M.; Liou, S.-J.; Lin, C.-Y.; Cheng, C.-Y.; Chang, Y.-W.; Lee, K.-R. Chem Mater 2002, 14, 154.
12. Yeh, J.-M.; Chen, C.-L.; Chen, Y.-C., Ma, C.-Y.; Lee, K.-R.; Wei, Y.; Li, S. Polymer 2002, 43, 2729.
13. Noh, M.-H.; Jang, L.-W.; Lee, D.-C. J Appl Polym Sci 1999, 74, 179.
14. Meier, L. P.; Sheldon, R. A.; Caseri, W. R.; Suter, U. W. Macromolecules 1994, 27, 1637.
15. Yano, K.; Usuki, A.; Okada, A. J Polym Sci Polym Chem Ed 1997, 35, 2289.
16. Wrobleski, D. A.; Benicewicz, B. C.; Thompson, K. G.; Byran, C. J. Polym Prepr (Am Chem Soc Div Polym Chem) 1994, 35, 265.
17. Lee, D. C.; Jang, L. W. J Appl Polym Sci 1996, 61, 1117.